Dressed Collective Qubit States and the Tavis-Cummings Model in Circuit QED

J. M. Fink,[1] R. Bianchetti,[1] M. Baur,[1] M. Göppl,[1] L. Steffen,[1] S. Filipp,[1] P. J. Leek,[1] A. Blais,[2] and A. Wallraff[1]

[1] *Department of Physics, ETH Zurich, CH-8093, Zurich, Switzerland.*
[2] *Département de Physique, Université de Sherbrooke, Sherbrooke, Québec J1K 2R1, Canada.*

(Dated: August 5, 2009)

We present an ideal realization of the Tavis-Cummings model in the absence of atom number and coupling fluctuations by embedding a discrete number of fully controllable superconducting qubits at fixed positions into a transmission line resonator. Measuring the vacuum Rabi mode splitting with one, two and three qubits strongly coupled to the cavity field, we explore both bright and dark dressed collective multi-qubit states and observe the discrete $\sqrt{N}$ scaling of the collective dipole coupling strength. Our experiments demonstrate a novel approach to explore collective states, such as the W-state, in a fully globally and locally controllable quantum system. Our scalable approach is interesting for solid-state quantum information processing and for fundamental multi-atom quantum optics experiments with fixed atom numbers.

PACS numbers: 42.50.Ct, 42.50.Pq, 03.67.Lx, 85.35.Gv

In the early 1950's, Dicke realized that under certain conditions a gas of radiating molecules shows the collective behavior of a single quantum system [1]. The idealized situation in which N two-level systems with identical dipole coupling are resonantly interacting with a single mode of the electromagnetic field was analyzed by Tavis and Cummings [2]. This model predicts the collective N-atom interaction strength to be $G_{\rm N} = g_{\rm j}\sqrt{N}$, where $g_{\rm j}$ is the dipole coupling strength of each individual atom j. In fact, in first cavity QED experiments the normal mode splitting, observable in the cavity transmission spectrum [3, 4], was demonstrated with on average $\bar{N} > 1$ atoms in optical [5, 6] and microwave [7] cavities to overcome the relatively weak dipole coupling $g_{\rm j}$. The $\sqrt{N}$ scaling has been observed in the regime of a small mean number of atoms $\bar{N}$ with dilute atomic beams [7–9] and fountains [10] crossing a high-finesse cavity. In these experiments, spatial variations of the atom positions and Poissonian fluctuations in the atom number inherent to an atomic beam [4, 8, 11] are unavoidable. In a different limit where the cavity was populated with a very large number of ultra-cold ^{87}Rb atoms [12] and more recently with Bose-Einstein condensates [13, 14] the $\sqrt{N}$ nonlinearity was also demonstrated. However, the number of interacting atoms is typically only known to about $\sim 10\%$ [13].

Here we present an experiment in which the Tavis-Cummings model is studied for a discrete set of fully controllable artificial atoms at fixed positions and with virtually identical couplings to a resonant cavity mode. The investigated situation is sketched in Fig. 1 a, depicting an optical analog where three two-state atoms are deterministically positioned at electric field antinodes of a cavity mode where the coupling is maximum. In our circuit QED [15, 16] realization of this configuration (Fig. 1 b), three transmon-type [17] superconducting qubits are embedded in a microwave resonator which contains a quantized radiation field. The cavity is realized as a coplanar waveguide resonator with a first harmonic full wavelength resonance frequency of $\omega_{\rm r}/2\pi = 6.729$ GHz and a photon decay rate of $\kappa/2\pi = 6.8$ MHz. The qubits are positioned at the antinodes of the first harmonic standing wave electric field. The transition frequency between ground $|g\rangle$ and first excited state $|e\rangle$ of qubit j, approximately given by $\omega_{\rm j} \approx \sqrt{8E_{\rm C_j}E_{\rm J_j}(\Phi_{\rm j})}/\hbar - E_{\rm C_j}/\hbar$, is controllable through the flux dependent Josephson energy $E_{\rm J_j}(\Phi_{\rm j}) = E_{\rm J\ max_j}|\cos(\pi\Phi_{\rm j}/\Phi_0)|$ [17]. Here $E_{\rm C_j}$ is the single electron charging energy, $E_{\rm J\ max_j}$ the maximum Josephson energy at flux $\Phi_{\rm j} = 0$ and Φ_0 the magnetic flux quantum. Independent flux control of each qubit is achieved by applying magnetic fields with three external miniature current biased coils (Fig. 2 a) where we take into account all cross-couplings by inverting the full coupling matrix. Optical images of the investigated sample are depicted in Fig. 2 b and c. The resonator was fabri-

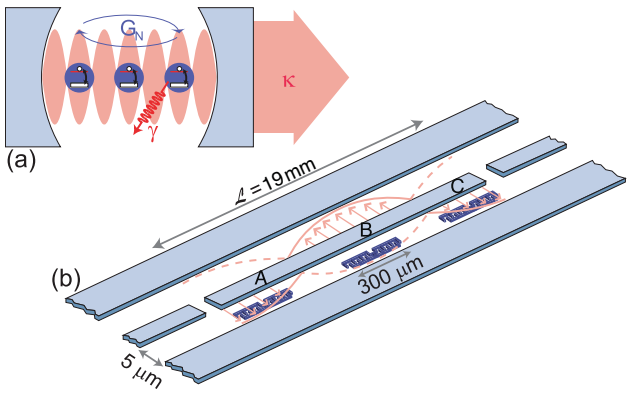

FIG. 1: Schematic of the experimental set-up. (a) Optical analog. Three two-state atoms are identically coupled to a cavity mode with photon decay rate κ, atomic energy relaxation rate γ and collective coupling strength $G_{\rm N}$. (b) Schematic of the investigated system. The coplanar waveguide resonator is shown in light blue, the transmon qubits A, B and C in violet and the first harmonic of the standing wave electric field in red.

cated employing optical lithography and Aluminum evaporation techniques on a Sapphire substrate. All qubits were fabricated with electron beam lithography and standard $Al/AlO_x/Al$ shadow evaporation techniques. Table I states the individual qubit parameters obtained from spectroscopic measurements.

The physics of our system is described by the Tavis-Cummings Hamiltonian [2]

$$\hat{\mathcal{H}}_{\rm TC} = \hbar\omega_{\rm r}\hat{a}^\dagger\hat{a} + \sum_j \left(\frac{\hbar}{2}\omega_{\rm j}\hat{\sigma}_{\rm j}^{\rm z} + \hbar g_{\rm j}(\hat{a}^\dagger\hat{\sigma}_{\rm j}^- + \hat{\sigma}_{\rm j}^+\hat{a})\right), \quad (1)$$

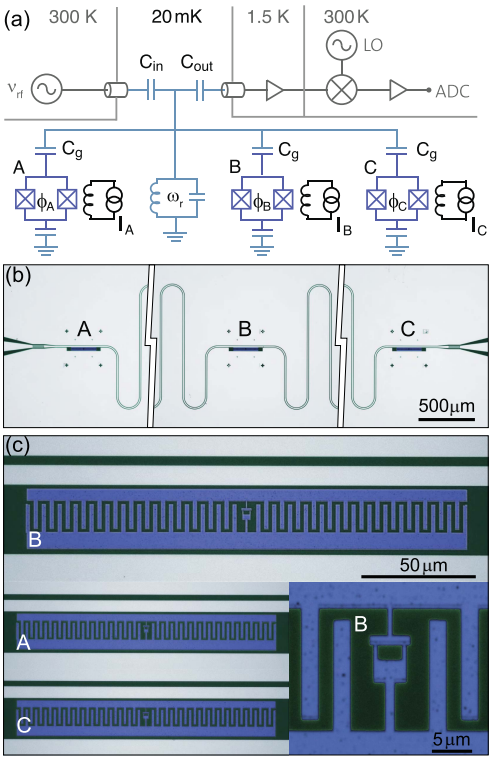

FIG. 2: Circuit diagram and false color optical images of the sample. (a) Simplified electrical circuit diagram of the experimental setup. The waveguide resonator operated at a temperature of 20 mK, indicated as LC oscillator with frequency ω_r, is coupled to input and output leads with the capacitors $C_{\rm in}$ and $C_{\rm out}$. Qubits A, B and C are controlled with external current biased coils ($I_{A,B,C}$) and coupled to the resonator via identical capacitors $C_{\rm g}$. A transmission measurement is performed by applying a measurement tone $\nu_{\rm rf}$ to the input port of the resonator, amplifying the transmitted signal and digitizing it with an analog-to-digital converter (ADC) after down-conversion with a local oscillator (LO) in a heterodyne detection scheme. (b) The coplanar microwave resonator is shown truncated in gray (substrate in dark green) and the locations of qubits A, B and C are indicated. (c) Top, magnified view of transmon qubit B (violet) embedded between ground plane and center conductor of the resonator. Bottom left, qubits A and C, of same dimensions as qubit B, are shown at reduced scale. Bottom right, magnified view of SQUID loop of qubit B.

where $g_{\rm j}$ is the coupling strength between the field and qubit j. $\hat{a}^\dagger$ and $\hat{a}$ are the creation and annihilation operators of the field, $\hat{\sigma}_{\rm j}^+$ and $\hat{\sigma}_{\rm j}^-$ are the corresponding operators acting on the qubit j, and $\hat{\sigma}_{\rm j}^{\rm z}$ is a Pauli operator. The ground state $|g,g,g\rangle \otimes |0\rangle$ of the three-qubit/cavity system is prepared by cooling the microchip to a temperature of 20 mK in a dilution refrigerator.

First we investigate the resonant coupling of the $|g\rangle$ to $|e\rangle$ transition of qubit A to the first harmonic mode of the resonator. We measure the anti-crossing between qubit A ($\nu_{\rm A}$) and the cavity ($\nu_{\rm r}$) by populating the resonator with much less than a photon on average. We record the resulting transmission spectrum T versus magnetic flux $\Phi_{\rm A}$ controlled detuning of qubit A (Fig. 3 a). Qubits B and C remain maximally detuned from the resonator at $\Phi_B = \Phi_C = \Phi_0/2$ where they do not affect the measurement. At finite detuning (left hand side of Fig. 3a) we observe a shift of the resonator spectrum which increases with decreasing detuning due to the dispersive interaction with qubit A.

On resonance ($\omega_{\rm j} = \omega_{\rm r}$) and in the presence of just one two level system ($N = 1$), Eq. (1) reduces to the Jaynes-Cummings Hamiltonian [18]. The eigenstates $|N, n\pm\rangle$ of this system in the presence of a single excitation $n = 1$ are the symmetric and anti-symmetric qubit-photon superpositions $|1, 1\pm\rangle = 1/\sqrt{2}\,(|g, 1\rangle \pm |e, 0\rangle)$ (Fig. 4 a) where the excitation is equally shared between qubit and photon. Accordingly, we observe a clean vacuum Rabi mode splitting spectrum formed by the states $|1, 1\pm\rangle$ (Fig. 3 b). From analogous measurements performed on qubits B and C (not shown) we obtain the single qubit coupling constants g_j listed in Tab. I. The coupling strengths are virtually identical with a scatter of only a few MHz. The strong coupling of an individual photon and an individual two-level system has been observed in a wealth of different realizations of cavity QED both spectroscopically [15, 19, 20] and in time-resolved experiments [21, 22]. The regime of multiple excitations n which proves field quantization in these systems has been reported both in the time resolved results cited above and more recently also in spectroscopic measurements [23–25].

In a next step, we maintain qubit A at degeneracy ($\nu_{\rm A} = \nu_{\rm r}$), where we observed the one-photon one-qubit doublet (see left of Fig. 3c). Qubit B remains far detuned

Qubit j	$E_{{\rm C}_j}/h$ (MHz)	$E_{{\rm J}_{{\rm max}\,j}}/h$ (GHz)	$g_{\rm j}/2\pi$(MHz)
A	283	224	83.7
B	287	226	-85.7
C	294	214	85.1

TABLE I: Qubit and qubit-resonator coupling parameters. The single electron charging energy $E_{{\rm C}_{\rm j}}$, the maximum Josephson energy $E_{{\rm J}_{\rm max\,j}}$ extracted from spectroscopic measurements and the coupling strengths $g_{\rm j}$ obtained from resonator transmission measurements for qubits A, B and C.

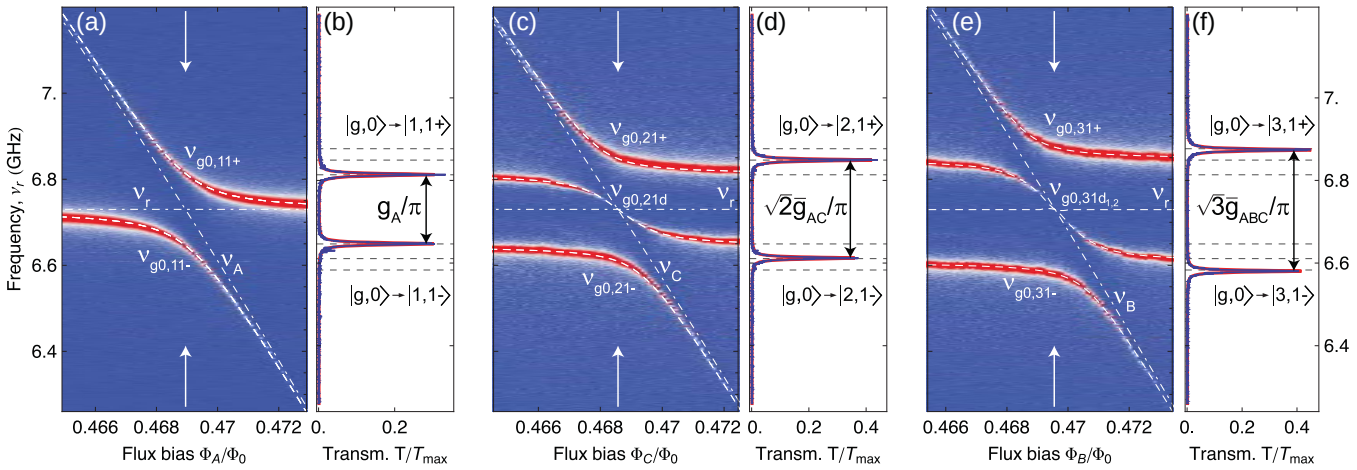

FIG. 3: Vacuum Rabi mode splitting with one, two and three qubits. (a) Measured resonator transmission spectrum T (blue, low and red, high transmission) versus normalized external flux bias Φ_A/Φ_0 of qubit A. Dash-dotted white lines indicate bare resonator ν_r and qubit ν_A frequencies and dashed white lines are calculated transition frequencies $\nu_{g0,Nn\pm}$ between $|g,0\rangle$ and $|N,n\pm\rangle$. (b) Resonator transmission T/T_{max} at degeneracy normalized to the maximum resonator transmission T_{max} measured at $\Phi_{A,B,C} = \Phi_0/2$ (not shown), as indicated with arrows in (a). Red line is a fit to two Lorentzians. (c) Resonator transmission spectrum T/T_{max} versus external flux bias Φ_C/Φ_0 of qubit C with qubit A degenerate with the resonator ($\nu_A = \nu_r$). (d) Transmission spectrum T/T_{max} at flux as indicated in (c). (e) Transmission spectrum versus flux Φ_B/Φ_0 with both qubits A and C at degeneracy ($\nu_A = \nu_C = \nu_r$). The white dashed line at frequency $\nu_{g0,31d_{1,2}} = \nu_r$ indicates the dark state occurring at degeneracy. (f) Transmission spectrum T/T_{max} at flux as indicated in (e).

($\Phi_B = \Phi_0/2$) for the entire measurement. Qubit C is then tuned through the already coupled states from lower to higher values of flux Φ_C. In this case, the doublet states $|1,1\pm\rangle$ of qubit A are found to be dispersively shifted due to non-resonant interaction with qubit C (Fig. 3 c). When both qubits and the resonator are exactly in resonance, the transmission spectrum T (Fig. 3 d) shows only two distinct maxima corresponding to the doublet $|2,1\pm\rangle = 1/\sqrt{2}\ |g,g\rangle \otimes |1\rangle \pm 1/2\ (|e,g\rangle + |g,e\rangle) \otimes |0\rangle$ with eigenenergies $\hbar(\omega_r \pm G_2)$. Here a single excitation is shared between one photon, with probability 1/2, and two qubits, with probability 1/4 each (Fig. 4 b). Both states have a photonic component and can be excited from the ground state $|g,g,g\rangle \otimes |0\rangle$ by irradiating the cavity with light. These are thus referred to as bright states. In general we expect $N + n = 3$ eigenstates for two qubits and one photon. The third state $|2,1d\rangle = 1/\sqrt{2}(|e,g\rangle - |g,e\rangle) \otimes |0\rangle$ with energy $\hbar\omega_r$ at degeneracy has no matrix element with a cavity excitation and is referred to as a dark state. Accordingly we observe no visible population in the transmission spectrum at frequency ν_r at degeneracy. In this regime the two qubits behave like one effective spin with the predicted [26] coupling strength $G_2 = \sqrt{2}\,\bar{g}_{AC}$ with $\bar{g}_{AC} = \sqrt{1/2(g_A^2 + g_C^2)}$, which is indicated by dashed black lines in Fig. 3 d. This prediction is in very good agreement with our measurement.

Following the same procedure, we then flux tune qubit B through the already resonantly coupled states of qubits A, C and the cavity ($\nu_A = \nu_C = \nu_r$), (Fig. 3 e). We observe the energies of three out of $N + n = 4$ eigenstates, the fourth one being dark, for a range of flux values Φ_B. Starting with the dark state $|2,1d\rangle$ at frequency ν_r and the doublet $|2,1\pm\rangle$ (left part of Fig. 3 e), the presence of qubit B dresses these states and shifts the doublet $|2,1\pm\rangle$ down in frequency. Again one of these states turns dark as it approaches degeneracy where it is entirely mixed with qubit B. At degeneracy we identify two bright doublet states $|3,1\pm\rangle = 1/\sqrt{2}\ |g,g,g\rangle \otimes |1\rangle \pm 1/\sqrt{6}\ (|e,g,g\rangle - |g,e,g\rangle + |g,g,e\rangle) \otimes |0\rangle$ (Fig. 4 c). The part of the states $|3,1\pm\rangle$ carrying the atomic excitation is a so called W-state, in which a single excitation is equally shared among

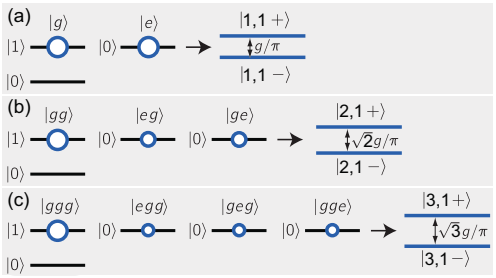

FIG. 4: Level diagram representing the total energy of (a) one (b) two and (c) three qubits resonantly coupled to a single photon. Bare energy levels of the qubits $|g\rangle$, $|e\rangle$ and the cavity $|0\rangle$, $|1\rangle$ are shown in black. The bright dressed energy levels $|N,n\pm\rangle$, with N the number of qubits, n the number of excitations and $\pm$ indicating the symmetry of the state, are illustrated in blue. The areas of the circles indicate the relative population of the bare states in the eigenstates $|N,n\pm\rangle$.

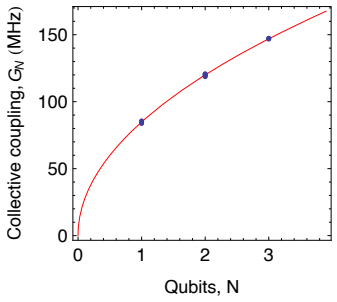

FIG. 5: Scaling of the collective dipole coupling strength. Measured coupling constants (blue dots) extracted from Fig. 3 and nine similar data sets and theoretical scaling (red line).

all N qubits [27]. Both $|3,1\pm\rangle$ states are clearly visible in the transmission spectrum shown in Fig. 3 f.

In addition, there are two dark states $|3,1d_1\rangle = 1/\sqrt{2}(|e,g,g\rangle - |g,g,e\rangle) \otimes |0\rangle$ and $|3,1d_2\rangle = 1/\sqrt{2}(|g,e,g\rangle + |g,g,e\rangle) \otimes |0\rangle$ which do not lead to resonances in the transmission spectrum at degeneracy. In general all $N+n-2$ dark states are degenerate at energy $\hbar\omega_r$. The symmetries of the dressed three-qubit states are determined by the signs of the coupling constants $g_A \approx -g_B \approx g_C$. While our measurement is not sensitive to the sign of coupling, it is a simple consequence of the phase shift of the electric field mode by π between the ends and the center of the resonator. Again, the observed transmission peak frequencies are in agreement with the calculated splitting of the doublet $G_3 = \sqrt{3}\,\overline{g}_{ABC}$ (dashed black lines in Fig. 3 f). Also at finite detunings the measured energies of all bright states are in excellent agreement with the predictions based on the Tavis-Cummings model (dashed white lines in Fig. 3 a,c,e) using the measured qubit and resonator parameters. We have also performed analogous measurements of all twelve one, two and three qubit anti-crossings (nine are not shown) and find equally good agreement.

In Fig. 5 all twelve measured coupling strengths (blue dots) for one, two and three qubits at degeneracy are plotted *vs.* N. Excellent agreement with the expected collective interaction strength $G_N = \sqrt{N}\,\overline{g}_{ABC}$ (red line) is found without any fit parameters and $\overline{g}_{ABC} = 84.8$ MHz.

Our spectroscopic measurements clearly demonstrate the collective interaction of a discrete number of quantum two-state systems mediated by an individual photon. All results are in good agreement with the predictions of the basic Tavis-Cummings model in the absence of any number, position or coupling fluctuations. The presented approach may enable novel investigations of super- and sub-radiant states of artificial atoms. Flux tuning on nanosecond timescales should furthermore allow the controlled generation of Dicke states [28, 29] and fast entanglement generation via collective interactions [30, 31], not relying on individual qubit operations. This could be used for quantum state engineering and an implementation of Heisenberg limited spectroscopy [32] in the solid state.

We thank T. Esslinger and A. Imamoğlu for discussions. This work was supported by SNF grant no. 200021-111899 and ETHZ. P. J. L. was supported by the EU with a MC-EIF. A. B. was supported by NSERC, CIFAR and the Alfred P. Sloan Foundation.

[1] R. H. Dicke, *Phys. Rev.* **93**, 99 (1954).
[2] M. Tavis and F. W. Cummings, *Phys. Rev.* **170**, 379 (1968).
[3] G. S. Agarwal, *Phys. Rev. Lett.* **53**, 1732 (1984).
[4] S. Leslie, N. Shenvi, K. R. Brown, D. M. Stamper-Kurn and K. B. Whaley, *Phys. Rev. A* **69**, 043805 (2004).
[5] M. G. Raizen, R. J. Thompson, R. J. Brecha, H. J. Kimble and H. J. Carmichael, *Phys. Rev. Lett.* **63**, 240 (1989).
[6] Y. Zhu *et al.*, *Phys. Rev. Lett.* **64**, 2499 (1990).
[7] F. Bernardot, P. Nussenzveig, M. Brune, J. M. Raimond and S. Haroche, *Europhys. Lett.* **17**, 33 (1992).
[8] J. J. Childs, K. An, M. S. Otteson, R. R. Dasari and M. S. Feld, *Phys. Rev. Lett.* **77**, 2901 (1996).
[9] R. J. Thompson, Q. A. Turchette, O. Carnal and H. J. Kimble, *Phys. Rev. A* **57**, 3084 (1998).
[10] P. Münstermann, T. Fischer, P. Maunz, P. W. H. Pinkse and G. Rempe, *Phys. Rev. Lett.* **84**, 4068 (2000).
[11] H. J. Carmichael and B. C. Sanders, *Phys. Rev. A* **60**, 2497 (1999).
[12] A. K. Tuchman *et al.*, *Phys. Rev. A* **74**, 053821 (2006).
[13] F. Brennecke *et al.*, *Nature* **450**, 268 (2007).
[14] Y. Colombe *et al.*, *Nature* **450**, 272 (2007).
[15] A. Wallraff *et al.*, *Nature* **431**, 162 (2004).
[16] R. J. Schoelkopf and S. M. Girvin, *Nature* **451**, 664 (2008).
[17] J. Koch *et al.*, *Phys. Rev. A* **76**, 042319 (2007).
[18] E. Jaynes and F. Cummings, *Proc. IEEE* **51**, 89 (1963).
[19] A. Boca *et al.*, *Phys. Rev. Lett.* **93**, 233603 (2004).
[20] G. Khitrova, H. M. Gibbs, M. Kira, S. W. Koch and A. Scherer, *Nat. Phys.* **2**, 81 (2006).
[21] M. Brune *et al.*, *Phys. Rev. Lett.* **76**, 1800 (1996).
[22] M. Hofheinz *et al.*, *Nature* **454**, 310 (2008).
[23] I. Schuster *et al.*, *Nat. Phys.* **4**, 382 (2008).
[24] J. M. Fink *et al.*, *Nature* **454**, 315 (2008).
[25] L. S. Bishop *et al.*, *Nat. Phys.* **5**, 105 (2009).
[26] C. E. López, H. Christ, J. C. Retamal and E. Solano, *Phys. Rev. A* **75**, 033818 (2007).
[27] W. Dür, G. Vidal and J. I. Cirac, *Phys. Rev. A* **62**, 062314 (2000).
[28] J. K. Stockton, R. van Handel and H. Mabuchi, *Phys. Rev. A* **70**, 022106 (2004).
[29] C. E. López, J. C. Retamal and E. Solano, *Phys. Rev. A* **76**, 033413 (2007).
[30] T. E. Tessier, I. H. Deutsch, A. Delgado and I. Fuentes-Guridi, *Phys. Rev. A* **68**, 062316 (2003).
[31] A. Retzker, E. Solano and B. Reznik, *Phys. Rev. A* **75**, 022312 (2007).
[32] D. Leibfried *et al.*, *Science* **304**, 1476 (2004).